Available online at www.sciencedirect.com
ScienceDirect
Chinese Journal of Natural Medicines 2019, **17**(9): 0650–0662
Chinese Journal of Natural Medicines

Exploration of the mechanisms of Ge Gen Decoction against influenza A virus infection

GENG Zi-Kai[1], LI Ya-Qun[1], CUI Qing-Hua[1, 2], DU Rui-Kun[1, 2], TIAN Jing-Zhen[1, 2*]

[1] *School of Pharmacy, Shandong University of Traditional Chinese Medicine, Jinan 250355, China;*
[2] *Collaborative Innovation Center for Antiviral Traditional Chinese Medicine, Jinan 250355, China*

Available online 20 Sep., 2019

[ABSTRACT] Ge Gen Decoction (GGD), a Traditional Chinese Medicine prescription, is mainly used to treat infectious respiratory diseases and can relieve the symptoms of influenza A virus (IAV) infection. However, the underlying mechanism of GGD against IAV infection remains unclear. In this study, we found that GGD had moderate anti-IAV activity *in vitro*. GGD was more effective when given before the viral infection and targeted the viral attachment and replication stages rather than the internalization stage. *In vivo*, GGD treatment reduced the virus titers of lung tissue significantly and improved the survival rate, lung index, and pulmonary histopathological changes in H1N1-infected mice. We observed the changes in several key immuno-related indexes in GGD administrated H1N1-infected mice with anti-IAV drug oseltamivir phosphate as the control. GGD treatment decreased the expression of TNF-α and improved Th1/Th2 immune balance to reduce the excessive immune response in H1N1-infected mice. Besides, the expression of the toll-like receptor 7 signaling pathway in H1N1-infected mice decreased after GGD treatment. Our results showed that GGD has anti-IAV activity and can modulate the immune system to relieve lung inflammation.

[KEY WORDS] Ge Gen Decoction; Traditional Chinese Medicine (TCM); H1N1; Antiviral; Immune regulation

[CLC Number] R965 **[Document code]** A **[Article ID]** 2095-6975(2019)09-0650-13

Introduction

Influenza is an infectious disease that poses a huge threat to human health. Currently, vaccines and antiviral medicines are the most effective therapies against influenza. However, IAV readily mutates, which allows drug-resistant mutants to emerge. Thus, it is vital to develop additional therapeutic strategies to tackle drug resistance.

As awareness of the intriguing bioactivity of many Chinese herbal extracts has grown, much research has focused on TCM [1]. TCM has made important contributions to the treatment of acute infectious diseases, such as SARS [2]. Because TCM uses extracts containing many bioactive ingredients, the antiviral mechanisms of TCM are different from those of common antiviral drugs, which contain a single chemical that usually targets a pathway vital for virus growth. Thus, understanding the unique modes of action of TCM against influenza infection may bring new insights to the fight against viral infections.

Ge Gen Decoction (GGD; kakkon-to in Japanese traditional medicine and Galgeun-tang in Korean traditional medicine) is a TCM prescription originating from the Treatise on Febrile Diseases. The prescription consists of *Pueraria lobata* (12 g·d^{-1}), *Ephedra sinica* (9 g·d^{-1}), *Cinnamomum cassia* (6 g·d^{-1}), *Glycyrrhiza uralensis* (6 g·d^{-1}), *Paeonia lactiflora* (6 g·d^{-1}), *Zingiber officinale* (9 g·d^{-1}), and *Ziziphus jujuba* (22 g·d^{-1}). GGD is mainly used to treat the common cold, influenza infection, and alleviate upper back pain. It is used widely in clinical practice in China and Japan, and there are no reports of adverse reactions. Several studies have found that treatment with GGD relieves influenza-like symptoms [3-5].

Although GGD has a curative effect on influenza infection, the underlying mechanism is unclear. GGD alleviated pulmonary inflammation and reduced mortality in IAV-infected mice; however, no effects on virus titers in lung tissue and bronchoalveolar lavage fluid (BALF) were seen [3, 6]. In contrast, another study indicated that GGD significantly re-

[Received on] 10-Jun.-2019
[Research funding] This work was supported by the Key R&D Project in Shandong Province (the Second Development of the Chinese Patent Medicine Ge Gen Decoction Granule, No. 2016CYJS08A01-8).
[*Corresponding author] Tel: 86-531-8962-8080, Fax: 86-531-8962-8080, E-mail: tianjingzhen@163.com
These authors have no conflict of interest to declare.

duced virus titers in BALF through improving natural killer cell activities in the primary phase of infection (day 2 after infection) [4].

Excessive immune activation, cytokine storm, and oxidative stress are the major causes of mortality in IAV-infected mice [7], and the imbalance of inflammation and anti-inflammation increases the pathogenicity of the influenza virus [8-9]. Some components of GGD have immunomodulatory and anti-inflammatory activities [10-15]; thus, in this study, we investigated the anti-inflammatory effects of GGD in IAV-infected mice. We examined the antiviral mechanism of GGD by measuring the direct anti-IAV H1N1 activities of GGD *in vitro* and *in vivo* and determining how GGD modulates the host immune system of IAV-infected mice to relieve the inflammation.

Materials and Methods

Reagents

Reference substances of Gallic acid (Lot: 1019C023), 3'-Hydroxypuerarin (Lot: 1019C02333), Puerarin (Lot: 1202A022), Paeoniflorin (Lot: 918B021), Daidzin (Lot: 1215A022), Daidzein (Lot: 715A021), Cinnamic acid (Lot: 510A022) and Glycyrrhizic acid (Lot: 419B021) were purchased from Solaibao technology Co., Ltd. (Beijing, China). Protocatechuic acid (Lot: Z30M6L1), Albiflorin (Lot: Y15D8H50784), 3'-Methoxypuerarin (Lot: P22A8F42194), Puerarin 6"-O-xyloside (Lot: P09J7F8771), Mirificin (Lot: P09J7F8770), Rutin (Lot: Y16M9S61523), Genistin (Lot: P09M8F31018), Ononin (Lot: R28O8F46957) and 6-Gingerol (Lot: Y02J9H52043) were bought from Yuanye Biotechnology Co., Ltd. (Shanghai, China). Ephedrine hydrochloride (Lot: 171241-201508) and Pseudoephedrine hydrochloride (Lot: 171237-201510) were obtained from the National Institutes for Food and Drug Control (Beijing, China). Acetonitrile and methanol (HPLC grade) were purchased from TEDIA (Ohio, USA). Formic acid (HPLC grade) was purchased from China National Pharmaceutical Group Corporation (Beijing, China). Oseltamivir Phosphate was purchased from MedChemExpress LLC (NJ, USA). The herbal materials of GGD were purchased from the Affiliated Hospital of Shandong University of Traditional Chinese Medicine (Jinan, Shandong, China) and authenticated by Professor XU Ling-Chuan (Shandong Traditional Chinese Medicine University, Jinan, China). The quality of these herbs reached the standards of Chinese Pharmacopoeia. The voucher specimens of the herbal materials were kept in the Collaborative Innovation Center.

Sample Preparation

According to the method in "Chinese Pharmacopoeia", *Pueraria lobate* (Wild.) (12 g), *Ephedra sinica* (9 g), *Cinnamomum cassia* (6 g), *Paeonia lactiflora* (6 g), *Glycyrrhiza uralensis* (6 g), *Zingiber officinale* (9 g) and *Ziziphus jujuba* (22 g) were decocted separately with 700 mL and 560 mL water for 30 minutes each time. The decoction was concentrated and freeze-dried to obtain the lyophilized extract powder (yield: 34.7%).

Stock solutions of the 19 reference substances were prepared by dissolving the powders in 50% methanol. The stock solutions were stored at 4 °C. The standard working solutions were obtained by mixing or diluting the stock solutions.

The lyophilized extract powder (equivalent to 1 g raw material) was dissolved in 10 mL 50% methanol. The solution was centrifuged at 7000 r·min^{-1} for 10 min. The supernatant was filtered through a 0.22 μm membrane before LC and LC/MS analysis.

HPLC-Q-TOF-MS/MS analysis and HPLC analysis

HPLC-Q-TOF-MS/MS analysis was performed on an Agilent 6520 Accurate-Mass Q-TOF LC/MS (Agilent Technologies, Santa Clara, CA, USA) equipped with an electrospray ionization source. Chromatographic separation was carried out on a ZORBAX SB-C_{18} column (5 μm, 4.6 mm × 250 mm, Agilent Technologies) with column temperature set at 30 °C. The mobile phase was composed of A (0.1% formic acid-water) and B (acetonitrile), a gradient elution was performed as follows: 0–30 min, 7% B; 30–45 min, 7%–11% B; 45–55 min, 11% B; 55–80 min, 11%–16% B; 80–120 min, 16%–30% B; 120–140 min, 30%–60% B. The sample injection volume was 10 μL, and the flow rate was 1.0 mL·min^{-1}. The DAD detector scanned from 200 to 400 nm, and the samples were detected at 245 nm. For MS detection, the operating parameters in both negative and positive ion modes were set as follows: drying gas (N_2) flow rate, 12 L·min^{-1}; drying gas temperature, 350 °C; capillary voltage, 3500 V; nebulizer pressure, 40 psi. The collision energy was automatically optimized according to the ion type. The MS range was set at *m/z* 100–1000.

An Agilent 1260 HPLC-DAD instrument (Agilent Technologies, CA, USA) was used for HPLC determination. The chromatographic separation conditions were the same as LC/MS mentioned above.

Cells and virus

Madin-Darby canine kidney (MDCK) cells were acquired from Cell Resource Center of Shanghai Academy of Life Sciences of the Chinese Academy of Sciences (Shanghai, China), which cultured in DMEM (Gibco, CA, USA) contained 10 % FBS (Gibco, CA, USA), 1000 U·mL^{-1} penicillin, and 100 μg·mL^{-1} streptomycin (Gibco, CA, USA). Infections were carried out in Opti-MEM containing 2 μg·mL^{-1} TPCK-Trypsin (Sigma-Aldrich, MO, USA).

Mouse-adapted influenza A virus (IAV) H1N1 [A/PR/8/34] was acquired from Chinese Center for Disease Control and Prevention (Beijing, China), which multiplied in the 10-day-old embryonated eggs. The 50% tissue culture infective dose ($TCID_{50}$) of the virus in the MDCK cells and 50% lethal dose (LD_{50}) of the virus in the mice were determined by the method of Reed-Muench [16] (1 × $10^{5.7}$ $TCID_{50}$/mL, 6.7 × 10^5 LD_{50}/mL).

Cytotoxicity assay

Various concentrations of GGD extract and Oseltamivir phosphate (OP) were inoculated into MDCK cells for 48 h.

The 50% cytotoxic concentration (CC_{50}) for MDCK cells was determined using a CCK-8 assay kit. The maximum drug concentration which caused cell mortality rate to be lower than 10% was chosen as drug non-cytotoxic concentration.

In vitro antiviral determination

OP was used as a reference control. Briefly, 1×10^4 cells/well were plated in 96-well plates and incubated for 18–24 h. The cells were supplemented with various concentrations of GGD or OP immediately after virus (TCID50/well) inoculation in triplicate. After 48 h, the virus inhibition rate was determined using CCK-8 assay [17] and calculated as Equation (1). The 50 % inhibitory concentration (IC_{50}) values of GGD and OP were calculated according to the Reed-Muench method [16].

$$\text{Virus Inhibition Rates} = \frac{OD_{\text{test}} - OD_{\text{model}}}{OD_{\text{control}} - OD_{\text{model}}} \times 100\% \quad (1)$$

Time-of-Addition assay

Antiviral activity of the GGD extract was examined before and after viral inoculation [18-19]. Briefly, the MDCK cells grown in 96-well plates were inoculated with 100 $TCID_{50}$/well virus. Various concentrations of GGD extract were supplemented at −4 h or −2 h (4 h or 2 h before viral inoculation), 2 h or 4 h (1 h or 2 h after viral inoculation). After 48 h incubation at 37 °C, the virus inhibition rate was determined as described above.

Attachment assay and internalization assay

The effect of GGD extract on viral attachment and internalization was also examined as described previously [18-19]. Briefly, for the attachment assay, the cells were pre-chilled at 4 °C for 1 h and inoculated with a mixture of virus (100 $TCID_{50}$/well) and different concentrations of GGD extract at 4 °C for 3 h. Then, the cells monolayer was firstly washed by PBS buffer (4 °C), then covered with fresh medium and incubated at 37 °C for another 48 h. For the internalization assay, the cells were pre-chilled at 4 °C for 1 h, then inoculated with the virus (100 $TCID_{50}$/well) and incubated at 4 °C for 3 h. The medium was replaced with fresh medium containing various concentrations of GGD extract. The cells were shifted to the culture at 37 °C for 1 h. Then, the cells monolayer was washed by PBS, covered with medium, and incubated at 37 °C for another 48 h.

The effect of GGD on the viral replication

The effect of GGD on the later stage of viral biosynthesis in a single infectious cycle was evaluated by qRT-PCR [17]. Briefly, the cells (3.5×10^5 cells/well) grown in 6 well plates were inoculated with virus (0.01 MOI). After incubation for 2 h at 37 °C, the medium was replaced with a fresh medium containing GGD (6.25 $mg \cdot mL^{-1}$) and OP (62.5 $\mu g \cdot mL^{-1}$) for three times. At 10 h post-infection, the viral RNA in the supernatants was isolated by using a Simply P Virus RNA Extraction Kit (Bio Flux, China) on a Bio-Rad CFX Connect apparatus. The primers are M-protein forward primer 5'-CTT CTAACCGAGGDCGAAAC-3' and M-protein reverse primer 5'-CGTCTACGCTGCAGTCCTC-3'. Recombinant plasmid including the M-protein gene of influenza virus (A/PR/8/34) was selected as a reference substance. In each experiment, a standard curve ($R^2 > 0.99$ within the range of 10^3 to 10^8 copies) was drawn to convert C_T into the number of viral-genome copies. The reaction conditions were as follows: 95 °C for 30 s, followed by 35 cycles of denaturation at 95 °C for 5 s, annealing and extension at 62 °C for 34 s.

In vivo anti-influenza virus experiments

Based on a previous report [20], female ICR mice (18 to 20 g) were inoculated intranasally with 20 μL of a viral suspension (5 LD_{50} or 0.8 LD_{50}) or PBS ($n = 6$) under anesthesia. The daily dosage of GGD extract (3.5 $g \cdot kg^{-1} \cdot d^{-1}$) or OP (21.2 $mg \cdot kg^{-1} \cdot d^{-1}$) was based on human-mouse equivalent dosage conversion. Mice were administered GGD, OP, or distilled water orally for 10 days from 3 days before infection. Mortality, weight and clinical features were monitored daily in the next two weeks. Mice with a weight loss of more than 20% were considered dead.

Another group of mice was inoculated with 0.8 LD_{50} of virus. From 3 days before infection, mice were administered GGD, OP, or distilled water orally. These mice were euthanized at the prescribed time. Lung and peripheral blood were harvested for further analysis. Based on previous reports, the viral load in the lung tissue was determined by RT-PCR assay [21].

Animals experiments were processed in line with approved regulations by Animal Protection and Use Committees, Shandong Traditional Chinese Medicine University (Approval: SDUTCM-2017024, 23 October 2017). Animals were maintained in the ABSL-2 laboratory, and all efforts were made to minimize animal suffering and the number of animals used in the experiment.

Pathological changes in lungs

The lung index assessed pulmonary edema. The pathological changes were observed on routine paraffin sections that were stained with hematoxylin (HE).

RT-PCR analysis

The total RNA of the lung tissue was isolated by using the RNAiso Plus reagent (Takara bio, China). The cDNA samples were prepared by using the PrimeScript RT reagent Kit (Takara bio, China). RT-PCR was performed with the SYBRs Premix Ex Tap TM II (Takara bio, China) on a Bio-Rad CFX Connect apparatus. The primers are described in Table 1. The reaction conditions were as follows: 95 °C for 30 s, followed by 35 cycles of denaturation at 95 °C for 5 s, annealing at 56 °C for 30 s and extension at 72 °C for 30 s. C_T value was analyzed using the comparative C_T ($\Delta\Delta C_T$) method. The results were normalized to GAPDH.

Western Blot analysis

Proteins were extracted from the lung tissue by RIPA buffer (Beyotime, Shanghai, China) containing PMSF (Beyotime, Shanghai, China) and Phosphatase inhibitor cocktail (Beyotime, Shanghai, China). A BCA protein concentration assay kit (Servicebio technology Co., Ltd., Wuhan, China) was used to measure protein concentration. Protein (40 μg) was separated by 8% (TLR7), 10% (virus-NP, MyD88,

TRAF6, IRF7, p-IRF7, and IKBα,) and 15% (IL-6, TNF-α, IFN-γ, and IL-4) SDS-PAGE. Proteins were transferred to PVDF membranes (0.22 μm, Millipore, Darmstadt, Germany). The membranes were separately incubated with various primary antibodies against IL-6, TNF-α (Proteintech Group, Illinois, USA), IFN-γ, IL-4 (Affinity Biosciences, Ohio, USA), virus-NP, TLR7, TRAF6, IKBα (Abcam, Shanghai, China), MyD88, IRF7, phospho-IRF7 (Ser477) (Affinity Biosciences, Ohio, USA), and β-actin (Abcam, Shanghai, China) at 4 °C overnight. The secondary antibody incubated the membranes for 30 min at 37 °C. Protein bands were detected by an ECL kit (Wuhan servicebio technology Co., Ltd., Wuhan, China) and visualized by an Alpha Innotech imaging system (San Leandro, CA, USA). If the different proteins on the blot need to be detected by the second set of specific probes, the primary and secondary antibodies will be cleaned with antibody stripping buffer (Beyotime, Jiangsu, China) and detected again. The results were normalized to β-actin.

Table 1 Primer sequence for RT-PCR

Target Gene	Direction	Sequence (5'- 3')
IL-1α	For	GTTCCTGACTTGTTTGAAGACC
	Rev	GTTGGACATCTTTGACGTTTCA
IL-6	For	GCTACCAAACTGGATATAATCAGGA
	Rev	CCAGGTAGCTATGGTACTCCAGAAC
TNF-α	For	TGTAGCCCACGTCGTAGC
	Rev	TTGAGATCCATGCCGTTG
IFN-γ	For	ATCTGGAGGAACTGGCAAAA
	Rev	TTCAAGACTTCAAAGAGTCTGAGG
IL-4	For	TACCAGGAGCCATATCCACGGATG
	Rev	TGTGGTGTTCTTCGTTGCTGTGAG
TLR7	For	CTGGAGTTCAGAGGCAACCATT
	Rev	GTTATCACCGGCTCTCCATAGAA
MyD88	For	CAGCGAGGDTTGCATCTTCTT
	Rev	TCACTTTCTTGGGGACTCAGG
TRAF6	For	GCAGTGAAAGATGACAGCGTGA
	Rev	TCCCGTAAAGCCATCAAGCA
IRF7	For	CTGGAAGCATTTCGGDCG
	Rev	CCTGTGTGGGCAGAGCA
NF-κB	For	ACGCGGATTCCTGTACACCT
	Rev	CAGGAGCTCCACAGGACAGA
GAPDH	For	CTTCTAACCGAGGDCGAAAC
	Rev	CGTCTACGCTGCAGTCCTC

Immunofluorescence labeling and flow cytometry

PBMCs were isolated from the peripheral blood by lymphocyte separation medium (Solarbio, Beijing, China). PBMCs were stimulated with phorbol myristate acetate (PMA, 30 ng·mL^{-1}, Beyotime, Shanghai, China) and ionomycin (1 μg·mL^{-1}, Beyotime, Shanghai, China) in the presence of monensin (1.7 μg·mL^{-1}, Beyotime, Shanghai, China) for 4 h. Then the cells were washed and resuspended in FACS staining buffer (PBS + 1% FBS). FC Receptor Blocker (BD Biosciences, NJ, USA) was used to block Fc receptors on the surface of cells. The cells were stained with anti-CD4-FITC (BD Biosciences, NJ, USA) antibodies in the dark at 4 °C for 30 min, then fixed with 4% Paraformaldehyde at 4 °C for 30 min. Next, the cells were washed and permeabilized by permeabilization solution (Solarbio, Beijing, China), then incubated with anti-IFN-γ-APC (BD Biosciences, NJ, USA) and anti-IL-4-PE (BD Biosciences, NJ, USA) antibodies at 4 °C for 1 h. Appropriate isotype controls were performed. The cells were washed by permeabilization solution and FACS staining buffer respectively, then suspended in FACS staining buffer and detected by flow cytometry (BD flow cytometer C6, BD Biosciences, NJ, USA).

Statistical Analysis

The results were expressed as the mean ± standard deviation (SD). Statistical analyses were performed using a two-tailed Independent-Samples t test. The Wilcoxon Mann-Whitney test conducted the statistical analysis of mortality. All data were analyzed by SPSS25 (IBM, Armonk, NY, USA).

Results and Discussion

Characterization of chemical constituents in GGD

By analyzing the retention time, molecular ion, and fragment ions of the chromatographic peaks, and comparing the results with reference substances and previous literature data [22-25], 31 compounds were identified in GGD (Table 2, Figs. 1a and 1b), which included nineteen flavonoids, three organic acids, three monoterpenoids, two triterpenoid saponins, two alkaloids, and two other types of compounds. The contents of seven components with antiviral, antimicrobial, and anti-inflammatory activities [10-14, 26-27] in GGD were determined by high-performance liquid chromatography (HPLC) as 0.63 mg·g^{-1} gallic acid, 21.46 mg·g^{-1} puerarin, 3.74 mg·g^{-1} paeoniflorin, 3.08 mg·g^{-1} daidzin, 0.48 mg·g^{-1} daidzein, 0.24 mg·g^{-1} cinnamic acid, and 1.8 mg·g^{-1} glycyrrhizic acid (Fig. 1c).

Table 2 Identification of chemical constituents in GGD

	Compound	Formula	Quasi-molecular	Theoretical value	Measured value	Error /ppm	MS/MS(m/z)
1[a]	Gallic acid[L]	$C_7H_6O_5$	$[M-H]^-$	169.0142	169.0145	1.78	125.02
2[a]	Protocatechuic acid[C/L]	$C_7H_6O_4$	$[M-H]^-$	153.0193	153.0195	1.31	109.03
3[a]	Ephedrine[E]	$C_{10}H_{15}NO$	$[M+H]^+$	166.1226	166.1223	1.81	148.11, 133.22, 115.05
4[a]	Pseudoephedrine[E]	$C_{10}H_{15}NO$	$[M+H]^+$	166.1226	166.1221	3.01	148.11, 133.08, 115.05
5	3′-Hydroxy-4′-*O*-glucosyl-Puerarin[P]	$C_{27}H_{30}O_{15}$	$[M+H]^+$	595.1657	595.166	0.50	433.14, 313.27, 148.11
6	Puerarin-4′-*O*-glucoside[P]	$C_{27}H_{30}O_{14}$	$[M+H]^+$	579.1708	579.1701	1.21	459.12, 417.12, 297.07
7	Kakkalide[P]	$C_{28}H_{32}O_{15}$	$[M+H]^+$	609.1814	609.1816	0.33	300.19, 285.28, 277.17, 247.13
8	Daidzein-4′, 7-diglucoside[P]	$C_{27}H_{30}O_{14}$	$[M+H]^+$	579.1708	579.1702	1.04	255.06, 417.11, 121.05

Continued

	Compound	Formula	Quasi-molecular	Theoretical value	Measured value	Error /ppm	MS/MS(*m/z*)
9[a]	3′-Hydroxypuerarin[P]	$C_{21}H_{20}O_{10}$	$[M+H]^+$	433.1129	433.1126	0.69	313.07, 261.08
10[a]	Puerarin[P]	$C_{21}H_{20}O_9$	$[M+H]^+$	417.118	417.1178	0.48	399.10, 381.09, 297.07
11[a]	Albiflorin[L]	$C_{23}H_{28}O_{11}$	$[M+H]^+$	481.1704	481.1704	0.00	341.09, 319.04, 197.08, 161.09, 133.08
12[a]	3′-Methoxypuerarin[P]	$C_{22}H_{22}O_{10}$	$[M+H]^+$	447.1286	447.1282	0.89	327.08, 342.16
13[a]	Puerarin 6”-*O*-xyloside[P]	$C_{26}H_{28}O_{13}$	$[M+H]^+$	549.1603	549.1607	0.73	417.11, 399.11, 366.24
14[a]	Mirificin[P]	$C_{26}H_{28}O_{13}$	$[M+H]^+$	549.1603	549.1614	2.00	417.11, 399.09, 351.14, 297.07, 267.26
15[a]	Paeoniflorin[L]	$C_{23}H_{28}O_{11}$	$[M+H]^+$	481.1704	481.1701	0.62	381.15, 341.11, 219.08
16[a]	Daidzin[P]	$C_{21}H_{20}O_9$	$[M+H]^+$	417.118	417.1182	0.48	255.23
17	3′-Methoxydaidzein[P]	$C_{16}H_{12}O_5$	$[M+H]^+$	285.0757	285.0751	2.11	270.05
18	Genistein-7-*O*-apiosyl-glucoside[P]	$C_{26}H_{28}O_{14}$	$[M+H]^+$	565.1552	565.1551	0.18	433.11, 415.19, 379.10, 313.07, 283.17
19[a]	Rutin[ZJ]	$C_{27}H_{31}O_{16}$	$[M+H]^+$	611.1607	611.1577	4.91	465.10, 303.05
20[a]	Genistin[P]	$C_{21}H_{20}O_{10}$	$[M+H]^+$	433.1129	433.1131	0.46	271.05
21	Formononetin-7-xylosyl-glucoside[P]	$C_{27}H_{30}O_{13}$	$[M+H]^+$	563.1759	563.1775	2.84	431.13, 413.19, 395.16, 311.08, 281.23
22	6''-*O*-malonyldaidzin[P]	$C_{24}H_{22}O_{12}$	$[M+H]^+$	503.1184	503.1204	3.98	459.21, 417.14, 255.06
23	Pueroside D[P]	$C_{24}H_{26}O_{10}$	$[M+H]^+$	475.1599	475.1597	0.42	313.10, 257.07, 207.06, 107.04
24[a]	Ononin[P]	$C_{22}H_{22}O_9$	$[M+H]^+$	431.1337	431.1336	0.23	269.08
25[a]	Daidzein[P]	$C_{15}H_{10}O_4$	$[M+H]^+$	255.0652	255.0652	0.00	199.06, 181.10, 153.13
26[a]	Cinnamic acid[C]	$C_9H_8O_2$	$[M-H]^-$	147.0451	147.0455	2.72	119.04, 117.05, 103.05
27	Benzoylpaeoniflorin[L]	$C_{30}H_{32}O_{12}$	$[M+COOH]^-$	629.1876	629.1851	3.97	583.18, 553.16, 535.21, 165.01, 121.01
28	Licorice saponin G2[G]	$C_{42}H_{62}O_{17}$	$[M+H]^+$	839.406	839.4056	0.48	487.34, 469.33
29[a]	Glycyrrhizic acid[G]	$C_{42}H_{62}O_{16}$	$[M+H]^+$	823.4111	823.4103	0.97	647.37, 471.34, 453.33
30	Formononetin[P]	$C_{16}H_{12}O_4$	$[M+H]^+$	269.0808	269.0801	2.60	254.17, 213.16
31[a]	6-Gingerol[ZR]	$C_{17}H_{26}O_4$	$[M-H]^-$	293.1758	293.1765	2.39	137.01

Not: P: *Pueraria lobate*, E: *Ephedra sinica*, C: *Cinnamomum cassia*, L: *Paeonia lactiflora*, G: *Glycyrrhiza uralensis*, ZR: *Zingiber officinale*, ZJ: *Ziziphus jujube*.
[a] compared with reference substances

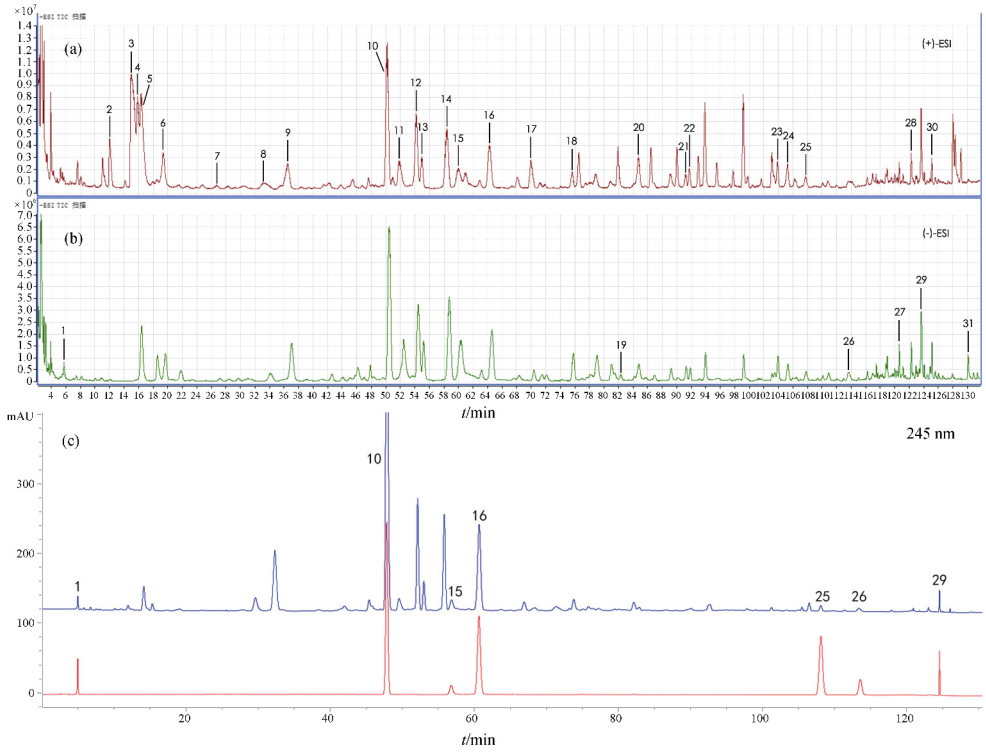

Fig. 1 Characterization of chemical constituents in GGD. (a) Total ion current chromatogram in positive ion mode. (b) Total ion current chromatogram in negative ion mode. (c) HPLC chromatograms of GGD (blue) and reference standards (red)

GGD extract showed antiviral activity against IAV in vitro

In vitro experiments showed that GGD and oseltamivir phosphate (OP) were dose-dependently effective against H1N1 (A/PR/8/34) in MDCK cells (Figs. 2a and 2b). The calculated IC_{50} values of GGD and OP were 1.81 mg·mL^{-1} and 13.20 μg·mL^{-1}, respectively. The CC_{50} of GGD was 10.88 mg·mL^{-1}, whereas that of OP was more than 250 μg·mL^{-1}.

A preliminary time-of-addition assay explored the possible antiviral mechanism of GGD. The drugs were added at different time points before and after viral inoculation. The activity of GGD against H1N1 in MDCK cells was dose-dependent and time-dependent (Fig. 2c). GGD was more effective when it was given before viral infection. The IC_{50} values were 1.42 mg·mL^{-1} (4 h before), 1.58 mg·mL^{-1} (2 h before), and 4.96 mg·mL^{-1} (2 h after). No noticeable difference was observed between 4 h before infection and 2 h before infection, which suggested that GGD might interfere with the attachment or internalization of the virus. A subsequent attachment assay confirmed this hypothesis. GGD inhibited viral attachment in a dose-dependent manner (Fig. 2d) with an IC_{50} of 2.59 mg·mL^{-1}. However, GGD did not affect viral internalization (Fig. 2e). Viral genome copies in the supernatants were analyzed by quantitative RT-PCR (qRT-PCR) to determine whether GGD affected the later stage of viral biosynthesis. At 10 h post-infection, the number of viral genome copies in the GGD treatment group was 5-fold lower than that in the model group (Fig. 2f).

In summary, GGD showed anti-IAV activity against H1N1 *in vitro* with an IC_{50} of 1.81 mg·mL^{-1} and targeted the viral attachment and replication stages rather than the internalization stage.

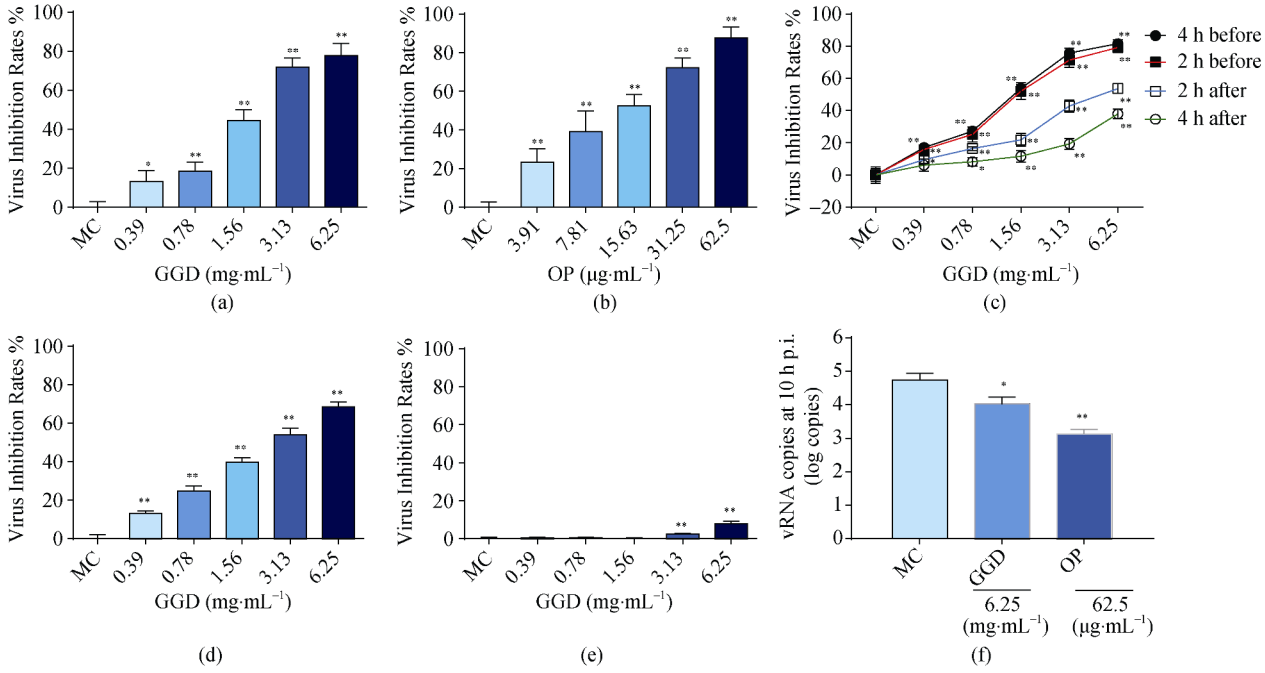

Fig. 2 ***In vitro*** **anti-IAV H1N1 assays. Antiviral activity of (a) GGD and (b) OP against H1N1** ***in vitro*****. (c) GGD extract showed dose-dependent and time-dependent activity against H1N1 in MDCK cells. (d) GGD inhibited viral attachment in a dose-dependent manner. (e) GGD did not affect viral internalization. (f) Effect of GGD on the later stage of viral biosynthesis in a single infectious cycle evaluated by qRT-PCR. Data are presented as the means ± SD (*n* = 3). $^{*}P < 0.05$, $^{**}P < 0.01$ *vs* the model group**

GGD increased the survival rate and decreased body weight loss of IAV-infected mice

Next, we investigated the effect of GGD in IAV-infected mice. The model group began to lose body weight, became inactive, and showed respiratory distress on day 3 post-infection (5 LD_{50}). The peak in the number of deaths appeared on day 6 to 7 post-infection. Although there were similar clinical features in the GGD group, they were less severe than those in the model group. Compared with the model group, mortality was significantly reduced by GGD treatment (3.5 g·kg^{-1}·d^{-1}, adult equivalent dose), whereas none died in the OP group (21.2 mg·kg^{-1}·d^{-1}, adult equivalent dose) (Fig. 3a).

Another group of mice was inoculated with a sub-lethal dose of H1N1 (0.8 LD_{50}). The body weight in the model group decreased markedly in the primary phase of infection and gradually recovered in the later phase (Fig. 3b). Compared with the model group, the body weight reduction was inhibited after GGD and OP treatment.

In summary, GGD reduced the mortality of mice infected with a lethal dose of virus and decreased the body weight loss of mice infected with a sublethal dose of virus. Although the protective effect of GGD was lower than that of OP for a lethal dose of H1N1 (5 LD_{50}), the curative effect of GGD was comparable to the OP for a sublethal dose of H1N1 (0.8 LD_{50}).

The results suggested that the infection dosage (0.8 and 5 LD_{50}) would affect the therapeutic efficacy of GGD. We reasoned that this might be the cause of the discrepancies surrounding the anti-IAV effects of GGD [3-6].

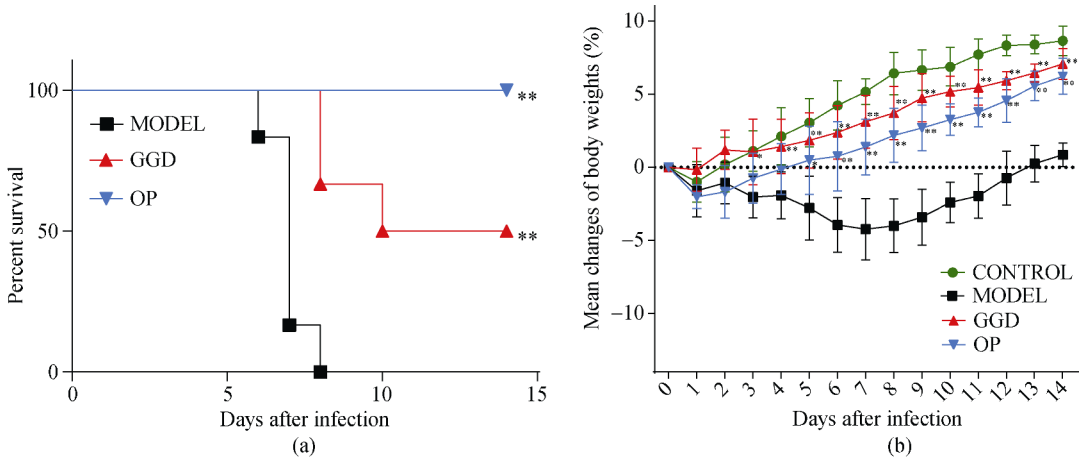

Fig. 3 Changes in mortality and body weight. (a) Mortality of mice inoculated with a lethal dose of H1N1 and treated with GGD (3.5 g·kg^{-1}·d^{-1}) or OP (62.5 μg·mL^{-1}) for 10 days from 3 days before infection. Mortality was monitored over two weeks (n = 6). (b) Changes in weight in mice inoculated with a sub-lethal dose of H1N1 and monitored over two weeks (n = 6). Data are presented as the means ± SD. $^{*}P < 0.05$, $^{**}P < 0.01$ *vs* the model group

GGD reduced virus titers in lung tissue and alleviated IAV-induced lung lesions

We measured the relative expression of H1N1 in the lung tissue of virus-infected mice (0.8 LD_{50}). An RT-PCR assay showed that the virus titers of lung tissue in the model group peaked on day 4 post-infection and fell again on day 6 post-infection ($P < 0.05$) (Fig. 4a). The virus titers of the lung tissue in the GGD and OP groups were significantly reduced ($P < 0.01$). On day 2 post-infection, the virus titers in the GGD group were higher than those in the OP group ($P < 0.05$); however, there was no significant difference in virus titers between in the GGD group and the OP group on day 4 and 6 post-infection ($P > 0.05$). The expression of the viral nucleoprotein in lung tissue on day 4 post-infection also confirmed this result (Figs. 4c and 4d).

These results indicated that influenza resolved on its own when mice were infected with a sub-lethal dose (0.8 LD_{50}) of H1N1. However, lung indexes (Fig. 4b) and pathological changes (Fig. 4e) in the model group showed that the immune system would inevitably cause inflammatory injury in the process of removing the virus, which is consistent with clinical observations. The treatment with GGD (3.5 g·kg^{-1}·d^{-1}) or OP (21.2 mg·kg^{-1}·d^{-1}) relieved the lung injury. Compared with the model group, GGD and OP treatment improved the lung indexes (Fig. 4b) and histological changes (Fig. 4e) on day 4 post-infection.

In summary, GGD had direct anti-IAV activity *in vitro* and *in vivo*. GGD treatment significantly reduced the virus titers in lung tissue and alleviated pathological damage in mice infected with H1N1 (0.8 LD_{50}). Some components in GGD have immunomodulatory and anti-inflammatory activities [10-15]. Thus, further studies are required to verify the anti-inflammatory and immunomodulatory hypothesis of GGD in the treatment of influenza.

GGD regulated the expression of IL-1α, IL-6, and TNF-α

The expression of cytokines in lung tissue was measured by RT-PCR and western blotting on day 4 post-infection. The RT-PCR assay showed that the mRNA expression of IL-1α in the model group was significantly higher than that in the control group. Compared with the model group, the expression of IL-1α mRNA was reduced after GGD and OP treatment, which is consistent with previous research [3] (Fig. 5a).

The RT-PCR assay indicated that the mRNA expression of IL-6 and TNF-α in the model group was significantly higher than that in the control group. The mRNA expression of IL-6 and TNF-α in the GGD and OP groups was lower than that in the model group (Figs. 5b and 5c). Notably, the expression of TNF-α mRNA in the GGD group was lower than that in the OP group ($P < 0.01$) (Fig. 5c). The protein expression of IL-6 and TNF-α was consistent with the mRNA data (Figs. 5d, 5e, and 5f).

The important pro-inflammatory cytokines IL-6 and TNF-α cause severe damage to the lungs during influenza infection [28], and the overexpression of pro-inflammatory cytokines increases the pathogenicity of influenza virus [9, 29]. Compared with the model group, the expression of IL-1α, IL-6, and TNF-α in lung tissue was decreased significantly after treatment with GGD and OP. However, compared with the OP group, the GGD group exhibited a unique immunomodulatory effect. The level of TNF-α in lung tissue after treatment with GGD was lower than that in the OP group. Because TNF-α is the main cytokine that causes acute lung injury [30], we propose that the decreased expression of TNF-α in the GGD group helped to relieve inflammatory injury in IAV-infected mice.

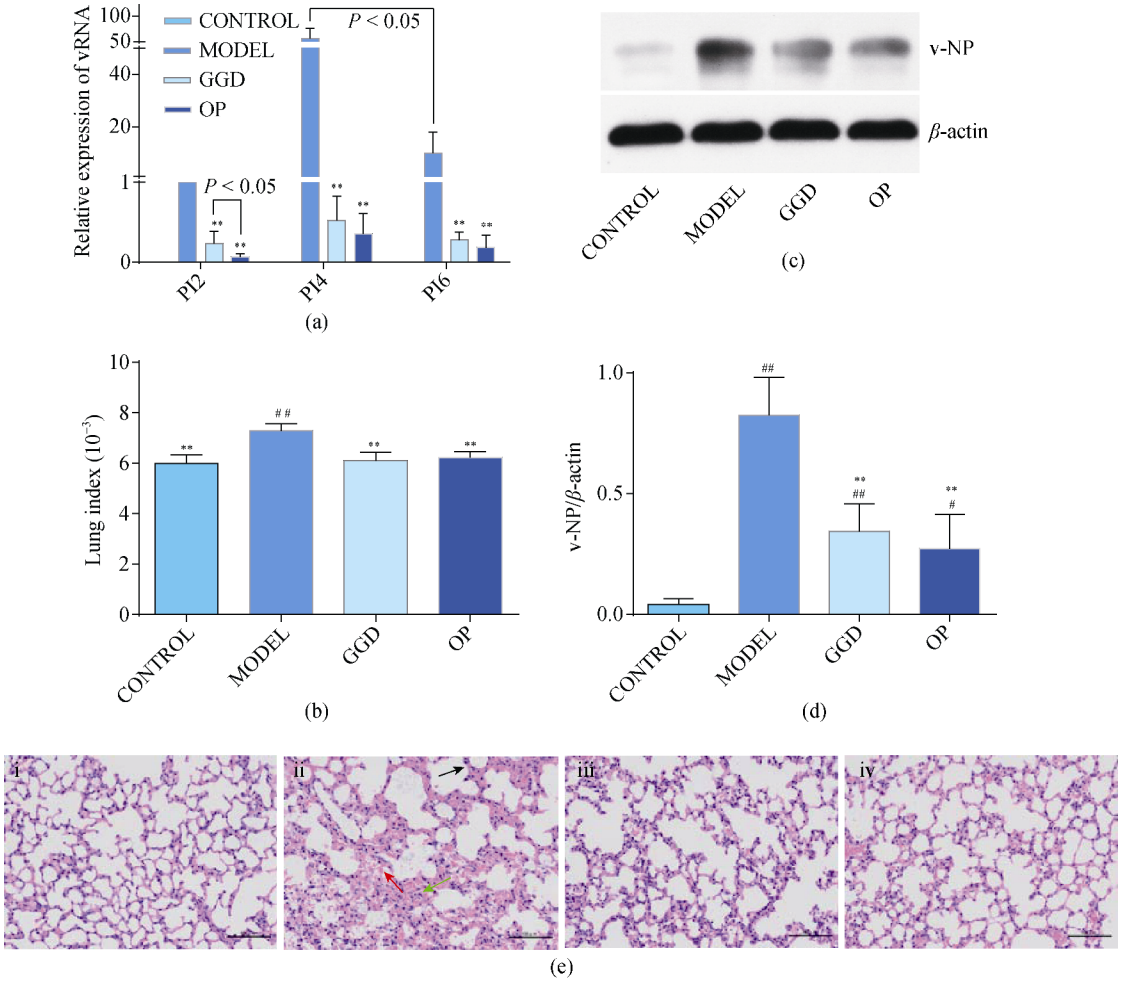

Fig. 4 Effects of GGD on virus titers in lung tissue and on lung lesions. (a) Virus titers in lung tissue measured by RT-PCR on day 2, 4, and 6 post-infection (0.8 LD_{50}) (n = 5). (b) Lung indexes on day 4 post-infection (0.8 LD_{50}) (n = 6). (c) Expression of viral nucleoprotein in lung tissue measured by western blotting on day 4 post-infection (0.8 LD_{50}) (n = 3). (d) Quantification of viral nucleoprotein expression relative to β-actin (n = 3). (e) Histological observation of lung tissue on day 4 post-infection (0.8 LD_{50}) (200 ×). (e-i) Alveolar structure of the control group is clear and interstitial alveolar walls show no inflammatory cells infiltration. (e-ii) Differences in the lung tissue of the model group, such as narrowed alveolar space (black arrow), thickened alveolar wall, lung congestion (red arrow), and infiltration of inflammatory cells (green arrow). The degree of lung lesions is reduced greatly in treated groups. Alveolar morphology following GGD (e-iii) and OP (e-iv) treatment is normal. Data are presented as the means ± SD. $^{*}P < 0.05$, $^{**}P < 0.01$ *vs* the model group. $^{\#}P < 0.05$, $^{\#\#}P < 0.01$ *vs* the control group

GGD improved the Th1/Th2 immune balance in H1N1-infected mice

To explore whether GGD exerts an anti-inflammatory effect by regulating the Th1/Th2 immune balance, we measured the expression of the Th1 and Th2 cytokines IFN-γ and IL-4, respectively, in lung tissue by RT-PCR and western blotting. Compared with the control group, the expression of IFN-γ was increased, whereas the expression of IL-4 was decreased in the model group on day 4 post-infection. However, compared with the model group, the expression of IFN-γ was decreased (Figs. 6a, 6c, and 6d), whereas the expression of IL-4 was increased (Figs. 6b, 6c, and 6e) after treatment with GGD and OP. Compared with the OP group, the level of IFN-γ in the GGD group was closer to those of the control group. This result indicates that GGD regulates the host immune system to maintain the balance of Th1/Th2.

To determine the effect of GGD on the Th1/Th2 balance, the percentages of CD4+IFN-γ+ and CD4+IL-4+ cells in peripheral lymphocytes were determined by flow cytometry. Compared with the control group, the Th1/Th2 ratio in the model group was significantly increased ($P < 0.01$), suggesting that the Th1/Th2 balance was pushed towards Th1 after infection (Figs. 6f, 6g, and 6h). Interestingly, compared with the OP group, the Th1/Th2 ratio in the GGD group was closer to that of the control group. These results suggest that the anti-inflammatory effect of GGD may be related to the improvement of the Th1/Th2 immune balance.

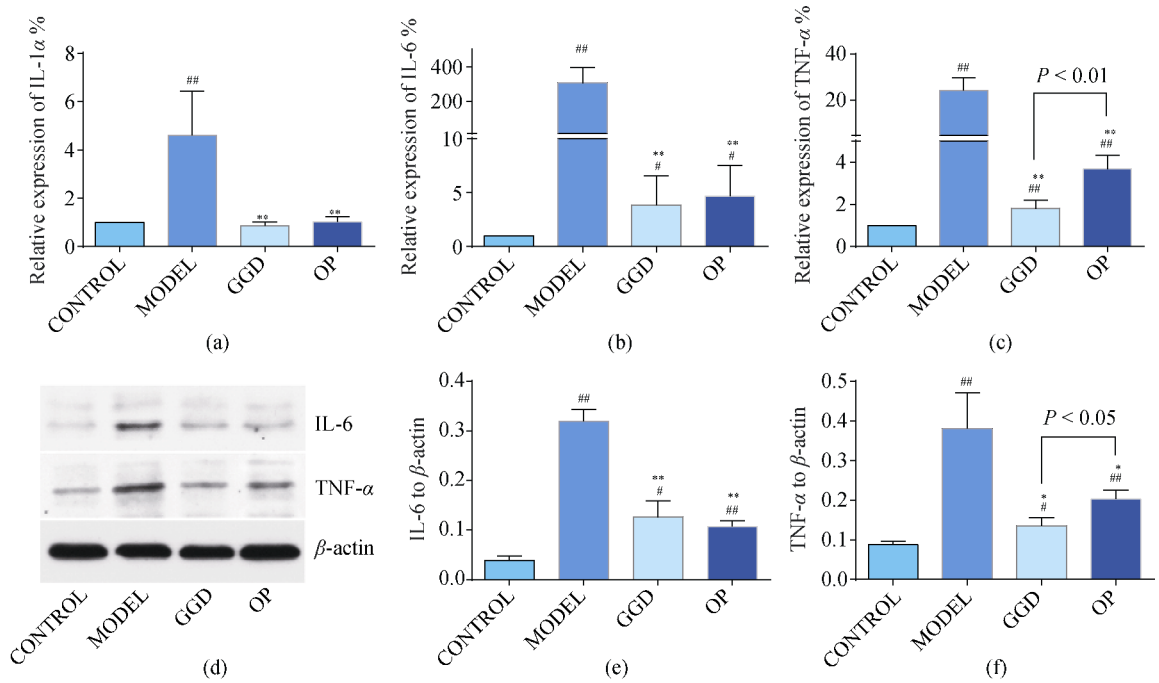

Fig. 5 Effects of GGD on the expression of IL-1*α*, IL-6, and TNF-*α* in lung tissue. mRNA expression of (a) IL-1*α*, (b) IL-6, and (c) TNF-*α* determined by RT-PCR on day 4 post-infection (*n* = 5). (d) Protein expression of IL-6 and TNF-*α* determined by western blotting on day 4 post-infection (*n* = 3). Quantification of (e) IL-6 and (f) TNF-*α* protein expression relative to *β*-actin. Data are presented as the means ± SD. $^{*}P < 0.05$, $^{**}P < 0.01$ *vs* the model group. $^{\#}P < 0.05$, $^{\#\#}P < 0.01$ *vs* the control group

Mouse CD4+ Th cells are divided into the Th1 and Th2 subgroups with different functions according to the types of cytokines they secrete [31]. In healthy individuals, the Th1/Th2 cell ratio maintains a dynamic balance. The Th1/Th2 imbalance is related to the induction of inflammation and the occurrence of various immune diseases [32]. Our study shows that the Th1/Th2 cell ratio was skewed toward Th1 after infection. Although cell-mediated anti-infective immune responses are essential in the clearance of the influenza virus [8, 33], Th1 cytokines, such as IFN-*γ* and TNF-*α*, also mediate inflammatory damage in the early stage of influenza [34]. IFN-*γ* and IL-4 are a pair of mutually inhibitory cytokines that indirectly reflect the degree of the Th1 and Th2 immune responses. The immunomodulation function of GGD can be inferred by comparing the changes in IFN-*γ* and IL-4 expression in the GGD and OP groups. Compared with the OP group, the level of IFN-*γ* in lung tissue and the CD4+IFN-*γ*+/CD4+IL-4+ ratio in the peripheral lymphocytes of the GGD group were closer to those of the control group. Thus, we believe that GGD regulates the immune system to maintain the Th1/Th2 balance, avoiding the over-activation of inflammation.

GGD affects the expression of the toll-like receptor 7 signaling pathway

Toll-like receptor 7 (TLR7) is a protein that recognizes the influenza virus and triggers an immune response [35]. Thus, we examined the effect of GGD on the TLR7 signaling pathway. We measured the mRNA and protein expression of key proteins in the TLR7 signaling pathway.

The RT-PCR assay showed that the expression of TLR7, myeloid differentiation primary response 88 (MyD88), TNF receptor associated factor 6 (TRAF6), and interferon regulatory factor 7 (IRF7) mRNA in the model group was significantly higher than that in the control group on day 4 post-infection (Fig. 7a). Compared with the model group, the mRNA expression of TLR7, MyD88, TRAF6, and IRF7 decreased after GGD and OP treatment. However, the expression of nuclear factor (NF)-*κ*B mRNA was similar in the GGD and OP groups.

Similar to mRNA levels, the expression of TLR7, MyD88, TRAF6, and phospho (P)-IRF7 protein in the model group increased, the P-IRF7/IRF7 ratio increased, and the expression of I*κ*B*α* protein decreased (Figs. 7b and 7c). Although there was no noticeable difference in the mRNA expression of NF-*κ*B among these groups, the reduced expression of I*κ*B*α* protein indicated that H1N1 triggered I*κ*B*α* degradation, indicating the activation of the NF-*κ*B pathway. Compared with the model group, the expression of TLR7, MyD88, TRAF6, and P-IRF7 protein in the GGD and OP groups was reduced, the P-IRF7/IRF7 ratio decreased, and the expression of I*κ*B*α* protein recovered. Moreover, the P-IRF7/IRF7 ratio in the GGD group was lower than that in the OP group ($P < 0.05$). However, the expression of total IRF7 protein was similar in the GGD and OP groups, which suggests that changes in the expression of P-IRF7 protein did not result from the change in total IRF7 protein.

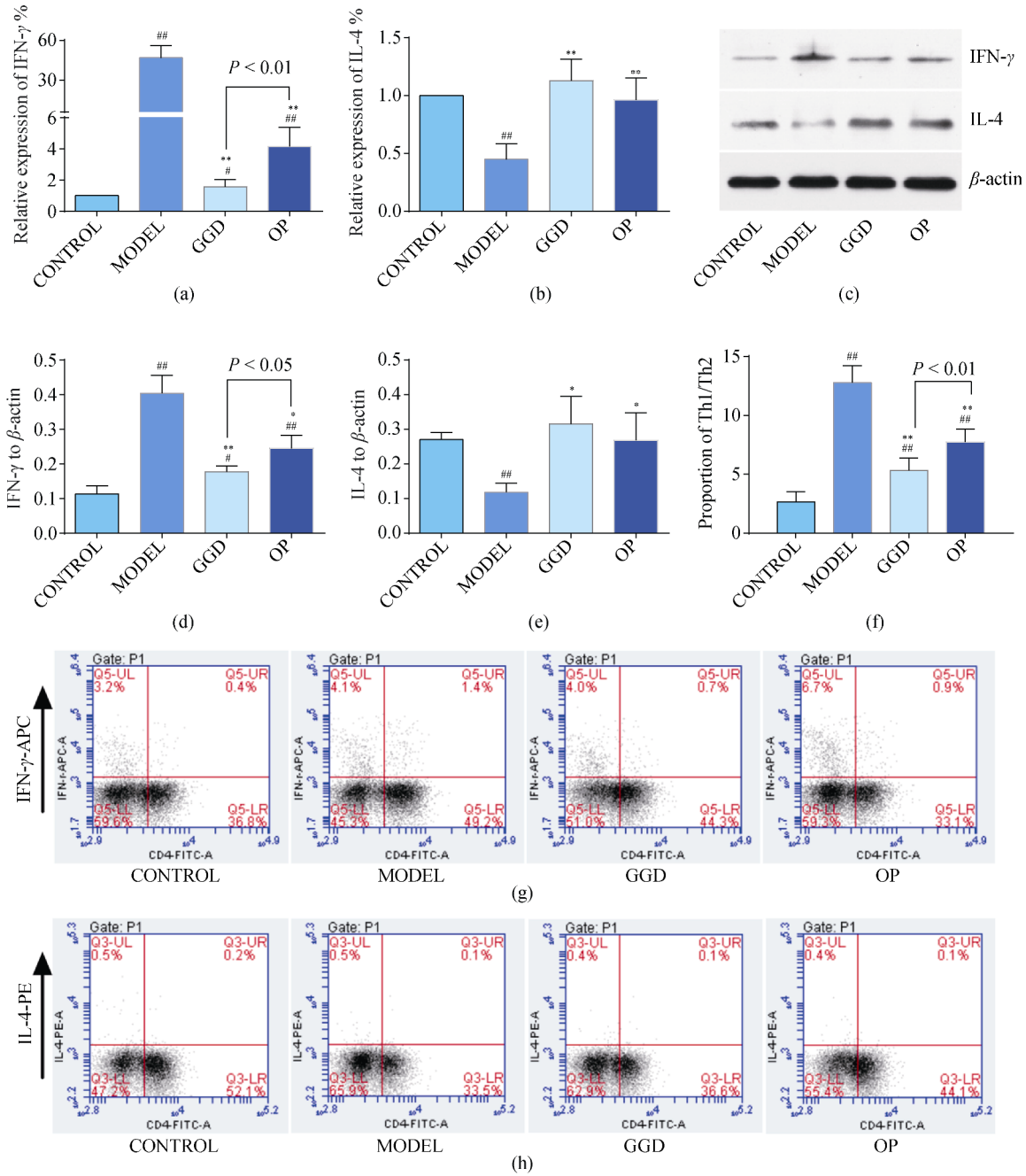

Fig. 6 Effects of GGD on Th1/Th2 balance. mRNA expression of (a) IFN-*γ* and (b) IL-4 determined by RT-PCR on day 4 post-infection (n = 5). (c) Protein expression of IFN-*γ* and IL-4 in lung tissue determined by western blotting (n = 3). Quantification of (d) IFN-*γ* and (e) IL-4 protein expression relative to *β*-actin. (f) Changes in the ratio of Th1/Th2 cells in peripheral lymphocytes determined by flow cytometry (n = 6). Representative FACS plots for (g) CD4+IFN-*γ*+ T cells and (h) CD4+IL-4+ T cells. Data are presented as the means ± SD. $^{*}P < 0.05$, $^{**}P < 0.01$ *vs* the model group. $^{\#}P < 0.05$, $^{\#\#}P < 0.01$ *vs* the control group

Toll-like receptors, which are pattern recognition receptors, play essential roles in recognizing pathogens and in inducing cascade signaling and immune responses [36-37]. TLR7 recognizes the single-stranded RNA of influenza viruses and triggers an immune response through a series of cascade reactions [35, 38]. The antiviral pathways mediated by the TLR7 signaling pathway may be TLR7-MyD88-TRAF6-NF-*κ*B and TLR7-MyD88-TRAF6-IRF7 [39]. However, the TLR7 signaling pathway also plays an essential role in the development of acute lung injury induced by the influenza virus [40]. The appropriate activation of the TLR7 signaling pathway is necessary for combating the infection. However, when these pathways are not properly controlled, the continuous and bulk release of inflammatory cytokines causes inflammatory injury [9, 41].

In the present study, the expression of TLR7, MyD88,

and TRAF6 and the activation levels of IRF7 and NF-κB in lung tissue increased significantly post-infection. After GGD treatment, the mRNA and protein expression of TLR7, MyD88, and TRAF6 decreased, and the activation levels of IRF7 and NF-κB decreased, which was consistent with the alleviation of pathological damage. In addition, the activation of IRF7 after GGD treatment was lower than that in the OP group, but this result requires further explanation.

In summary, we focused on the anti-inflammatory and immunomodulatory activities of GGD. By comparing several immune-related indexes in the GGD and OP groups, we found that GGD treatment decreased the expression of TNF-α to relieve lung injury. GGD treatment also regulated the balance of Th1/Th2 to alleviate inflammation. In addition, GGD treatment decreased the level of IRF7 activation, although the reason for this remains unclear.

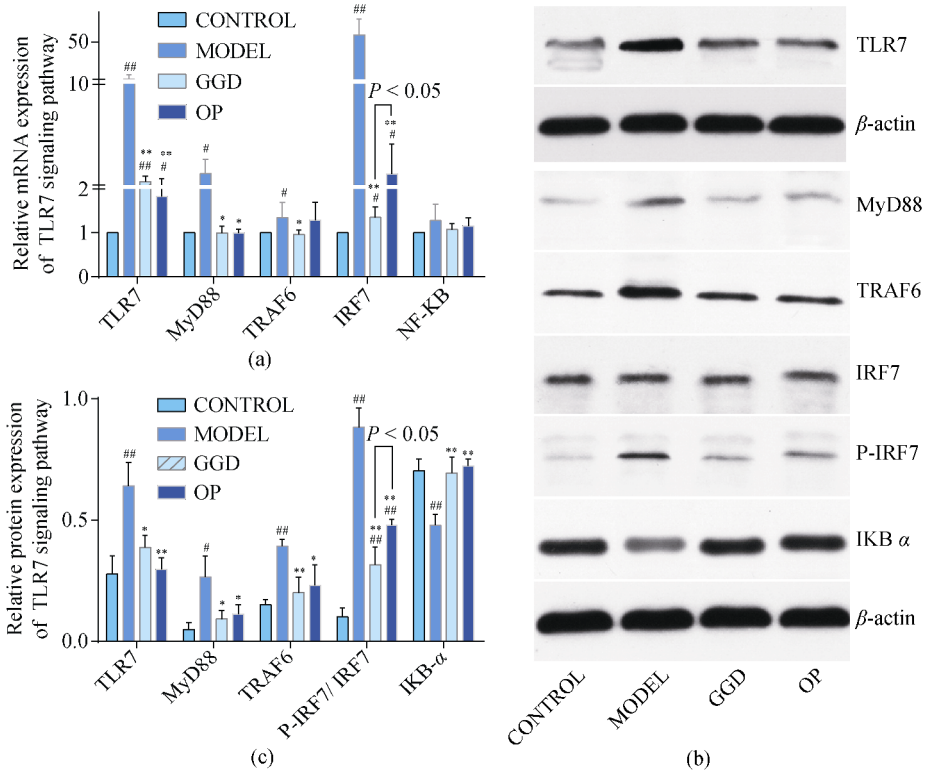

Fig. 7 mRNA and protein expression of the TLR7 signaling pathway in lung tissue. (a) Expression of TLR7, MyD88, TRAF6, IRF7, and NF-κB mRNA in lung tissue (n = 5). (b) Western blot of the protein expression of TLR7, MyD88, TRAF6, IRF7, P-IRF7, and IκBα in lung tissue (n = 3). (c) Quantification of TLR7, MyD88, TRAF6, P-IRF7/IRF7, and IκBα protein expression relative to β-actin. Data are presented as the means ± SD. $^{*}P < 0.05$, $^{**}P < 0.01$ *vs* the model group. $^{\#}P < 0.05$, $^{\#\#}P < 0.01$ *vs* the control group

Conclusions

GGD has been used in clinical practice for over 2000 years; however, we know little about its pharmacological mechanism in treating influenza infection. We demonstrated that GGD possesses anti-IAV H1N1 activity *in vitro* and *in vivo*. In addition, GGD downregulated the expression of TNF-α proinflammatory cytokines, regulated Th1/Th2 immune balance, reduced inflammation, and improved the prognosis in mice infected with H1N1. The TLR7 signaling pathway was also involved in the immunoregulation of GGD treatment. Our results indicate that GGD may be useful as an anti-IAV medicine owing to its unique anti-inflammatory and immunomodulatory activities.

Acknowledgments

We thank the professor RONG Li-Jun (The University of Illinois at Chicago, Chicago, USA) for providing the recombinant plasmid including M-protein gene of influenza virus. We thank professors YANG Yong and ZHANG Ying-Ying for valuable suggestions in the design of the experiments.

References

[1] Pan SY, Zhou SF, Gao SH, *et al*. New perspectives on how to discover drugs from herbal medicines: CAM's outstanding contribution to modern therapeutics [J]. *Evid Based Complement Alternat Med*, 2013, **2013**: 627375.

[2] Liu X, Zhang M, He L, *et al*. Chinese herbs combined with Western medicine for severe acute respiratory syndrome (SARS) [J]. *Cochrane Database Syst Rev*, 2012, **10**: Cd004882.

[3] Kurokawa M. Kakkon-to suppressed interleukin-1α production responsive to interferon and alleviated influenza infection in mice [J]. *J Tradit Med*, 1996, **13**: 201-209.

[4] Kurokawa M, Tsurita M, Brown J, *et al.* Effect of interleukin-12 level augmented by Kakkon-to, a herbal medicine, on the early stage of influenza infection in mice [J]. *Antiviral Res*, 2002, **56**(2): 183-188.

[5] Song J, Han Q, Qiao C, *et al.* Simultaneous determination of multiple marker constituents in concentrated Gegen Tang granule by high performance liquid chromatography [J]. *Chin Med*, 2007, **2**: 7.

[6] Nagai T, Yamada H. *In vivo* anti-influenza virus activity of kampo (Japanese herbal) medicine "sho-seiryu-to" and its mode of action [J]. *Int J Immunopharmacol*, 1994, **16**(8): 605-613.

[7] Hu Y, Jin Y, Han D, *et al.* Mast cell-induced lung injury in mice infected with H5N1 influenza virus [J]. *J Virol*, 2012, **86**(6): 3347-3356.

[8] Eichelberger M, Allan W, Zijlstra M, *et al.* Clearance of influenza virus respiratory infection in mice lacking class I major histocompatibility complex-restricted CD8+ T cells [J]. *J Exp Med*, 1991, **174**(4): 875-880.

[9] Loo YM, Jr GM. Fatal immunity and the 1918 virus [J]. *Nature*, 2007, **445**(7125): 267.

[10] Meng H, Fu G, Shen J, *et al.* Ameliorative effect of daidzein on cisplatin-induced nephrotoxicity in mice via modulation of inflammation, oxidative stress, and cell death [J]. *Oxid Med Cell Longev*, 2017, **2017**: 3140680.

[11] Xiao F, Cui H, Zhong X. Beneficial effect of daidzin in dry eye rat model through the suppression of inflammation and oxidative stress in the cornea [J]. *Saudi J Biol Sci*, 2018, **25**(4): 832-837.

[12] Wang YM, Du GQ. Glycyrrhizic acid prevents enteritis through reduction of NFkappaB p65 and p38MAPK expression in rat [J]. *Mol Med Rep*, 2016, **13**(4): 3639-3646.

[13] Li H, Jiao Y, Xie M. Paeoniflorin ameliorates atherosclerosis by suppressing TLR4-Mediated NF-kappaB activation [J]. *Inflammation*, 2017, **40**(6): 2042-2051.

[14] Wei SY, Chen Y, Xu XY. Progress on the pharmacological research of puerarin: a review [J]. *Chin J Nat Med*, 2014, **12**(6): 407-414.

[15] Wu Z, Kong X, Zhang T, *et al.* Pseudoephedrine/ephedrine shows potent anti-inflammatory activity against TNF-alpha-mediated acute liver failure induced by lipopolysaccharide/D-galactosamine [J]. *Eur J Pharmacol*, 2014, **724**: 112-121.

[16] Chen GL, Lamirande EW, Yang CF, *et al.* Evaluation of replication and cross-reactive antibody responses of H2 subtype influenza viruses in mice and ferrets [J]. *J Virol*, 2010, **84**(15): 7695-7702.

[17] Jin J, Chen S, Wang D, *et al.* Oroxylin A suppresses influenza A virus replication correlating with neuraminidase inhibition and induction of IFNs [J]. *Biomed Pharmacother*, 2018, **97**: 385-394.

[18] Ma Q, Yu Q, Xing X, *et al.* San Wu Huangqin Decoction, a Chinese herbal formula, inhibits influenza a/PR/8/34 (H1N1) virus infection *in vitro* and *in vivo* [J]. *Viruses*, 2018, **10**(3): 117.

[19] Wang KC, Chang JS, Chiang LC, *et al.* Sheng-Ma-Ge-Gen-Tang (Shoma-kakkon-to) inhibited cytopathic effect of human respiratory syncytial virus in cell lines of human respiratory tract [J]. *J Ethnopharmacol*, 2011, **135**(2): 538-544.

[20] Nagai T, Kataoka E, Aoki Y, *et al.* Alleviative effects of a kampo (a Japanese herbal) medicine "Maoto (Ma-Huang-Tang)" on the early phase of influenza virus infection and its possible mode of action [J]. *Evid Based Complement Alternat Med*, 2014, **2014**: 187036.

[21] Deng L, Pang P, Zheng K, *et al.* Forsythoside a controls influenza a virus infection and improves the prognosis by inhibiting virus replication in mice [J]. *Molecules*, 2016, **21**(5): 524

[22] Lv XJ, Sun Z, Wang PL, *et al.* Chemical profiling and quantification of Dan-Deng-Tong-Nao-capsule using ultra high performance liquid chromatography coupled with high resolution hybrid quadruple-orbitrap mass spectrometry [J]. *J Pharm Biomed Anal*, 2018, **148**: 189-204.

[23] Yan Y, Chai CZ, Wang DW, *et al.* HPLC-DAD-Q-TOF-MS/MS analysis and HPLC quantitation of chemical constituents in traditional Chinese medicinal formula Ge-Gen Decoction [J]. *J Pharm Biomed Anal*, 2013, **80**: 192-202.

[24] Bai X, Qu J, Lu J, *et al.* Pharmacokinetics of kakkalide and its main metabolites in rat plasma determined by HPLC-DAD and LC-MS_n [J]. *J Chromatogr B Analyt Technol Biomed Life Sci*, 2011, **879**(5-6): 395-402.

[25] Tao Y, Xu X, Yan J, *et al.* A sensitive UPLC-MS/MS method for simultaneous determination of polyphenols in rat plasma: Application to a pharmacokinetic study of dispensing granules and standard decoction of *Cinnamomum cassia* twigs [J]. *Biomed Chromatogr*, 2019: e4534.

[26] Wang Y, Sun Y, Wang J, *et al.* Antifungal activity and action mechanism of the natural product cinnamic acid against *Sclerotinia sclerotiorum* [J]. *Plant Dis*, 2019: Pdis08181355re.

[27] Lee JH, Oh M, Seok JH, *et al.* Antiviral effects of black Raspberry (*Rubus coreanus*) seed and its gallic acid against influenza virus infection [J]. *Viruses*, 2016, **8**(6): 157

[28] Zhang Y, Acuna CL, Switzer KC, *et al.* Corrective effects of interleukin-12 on age-related deficiencies in IFN-gamma production and IL-12Rbeta2 expression in virus-specific CD8+ T cells [J]. *J Interferon Cytokine Res*, 2000, **20**(2): 235.

[29] Uno Y, Usui T, Soda K, *et al.* The pathogenicity and host immune response associated with H5N1 highly pathogenic avian influenza virus in quail [J]. *J Vet Med Sci*, 2012, **75**(4): 451-457.

[30] Aldridge JR Jr, Moseley CE, Boltz DA, *et al.* TNF/iNOS-producing dendritic cells are the necessary evil of lethal influenza virus infection [J]. *Proc Natl Acad Sci U S A*, 2009, **106**(13): 5306-5311.

[31] Mosmann TR, Cherwinski H, Bond MW, *et al.* Two types of murine helper T cell clone. I. Definition according to profiles of lymphokine activities and secreted proteins. 1986 [J]. *J Immunol*, 2005, **175**(1): 5-14.

[32] O'Shea JJ, Paul WE. Mechanisms underlying lineage commitment and plasticity of helper CD4+ T cells [J]. *Science*, 2010, **327**(5969): 1098-1102.

[33] Bender BS, Croghan T, Zhang L, *et al.* Transgenic mice lacking class I major histocompatibility complex-restricted T cells

have delayed viral clearance and increased mortality after influenza virus challenge [J]. *J Exp Med*, 1992, **175**(4): 1143-1145.

[34] Hussell T, Pennycook A, Openshaw PJ. Inhibition of tumor necrosis factor reduces the severity of virus-specific lung immunopathology [J]. *Eur J Immunol*, 2001, **31**(9): 2566-2573.

[35] Lund JM, Alexopoulou L, Sato A, *et al.* Recognition of single-stranded RNA viruses by Toll-like receptor 7 [J]. *P Nat Acad Sci USA*, 2004, **101**(15): 5598-5603.

[36] Opitz B, Van LV, Eitel J, *et al.* Innate immune recognition in infectious and noninfectious diseases of the lung [J]. *Am J Respir Crit Care Med*, 2010, **181**(12): 1294-1309.

[37] Yamada S, Shimojima M, Narita R, *et al.* RIG-I-Like receptor and Toll-Like receptor signaling pathways cause aberrant production of inflammatory cytokines/chemokines in a severe fever with thrombocytopenia syndrome virus infection mouse model [J]. *J Virol*, 2018, **92**(13): e02246-17

[38] Casanova JL, Abel L, Quintana-Murci L. Human TLRs and IL-1Rs in host defense: natural insights from evolutionary, epidemiological, and clinical genetics [J]. *Annu Rev Immunol*, 2011, **29**(1): 447.

[39] Tamura T, Yanai H, Savitsky D, *et al.* The IRF family transcription factors in immunity and oncogenesis [J]. *Annu Rev Immunol*, 2008, **26**: 535-584.

[40] To EE, Broughton BRS, Hendricks KS, *et al.* Influenza A virus and TLR7 activation potentiate NOX2 oxidase-dependent ROS production in macrophages [J]. *Free Radical Res*, 2014, **48**(8): 940.

[41] Cholletmartin S, Montravers P, Gibert C, *et al.* State of activation of polynuclear neutrophils and cytokines in acute respiratory distress syndrome in adults [J]. *Pathol Biol*, 1993, **41**(8 Pt 2): 833.

Cite this article as: GENG Zi-Kai, LI Ya-Qun, CUI Qing-Hua, DU Rui-Kun, TIAN Jing-Zhen. Exploration of the mechanisms of Ge Gen Decoction against influenza A virus infection [J]. *Chin J Nat Med*, 2019, **17**(9): 650-662.